IEEE Access
Multidisciplinary | Rapid Review | Open Access Journal

Received August 11, 2018, accepted October 2, 2018, date of publication November 9, 2018, date of current version December 3, 2018.

Digital Object Identifier 10.1109/ACCESS.2018.2876886

Modeling of Multilayered Power/Ground Planes Based on Resonant Cavity Algorithm

JUN WANG, JIANMIN LU, XIUQIN CHU, YANG LIU, AND YUSHAN LI
Key Laboratory of High-Speed Circuit Design and EMC, Ministry of Education, Xidian University, Xi'an 710071, China

Corresponding author: Jianmin Lu (jmlu@xidian.edu.cn)

This work was supported in part by the National Natural Science Foundation of China under Grants 61871453 and 61501345 and in part by the Open Funds of the Key Laboratory of High-Speed Circuit Design and EMC under Grants 2017KFKT/B10 and 2017KFKT/B03.

ABSTRACT Based on the resonant cavity algorithm, a method is presented to model the multilayered power/ground planes with stitching vias at the high-speed packages and the printed circuit board. A multilayered structure can be seen as a combination of two basic units: adjacent planes with a different reference voltage and that with the same reference voltage. Then, the behaviors of the switching current in and the physics-based models for the multilayered power/ground planes with different basic units are presented. By analyzing the influence of stitching vias to the return path of the switching current in the multilayered structure, it is obtained that the remainder plane pairs act as a multiport load to the plane pair where the current load is located on. The algorithm for a plane pair with a multiport load is presented on the basis of the resonant cavity algorithm to efficient mode the multilayered power/ground planes. At the same time, this modeling method can be used in auto-decoupling design to consider the placements of decoupling capacitors. The modeling method is corroborated by the comparison with a 3-D electromagnetic commercial tool with wideband Z-parameter computation from dc to 10 GHz.

INDEX TERMS Multilayer, power distribution network, power integrity, resonant cavity model.

I. INTRODUCTION

In modern high speed digital circuits, the design of power distribution network (PDN) is becoming a challenging task to supply of clean power to the switching circuits. The process dimension of integrated circuits (IC) has been aggressively reduced to yield smaller transistors, higher integration density, and faster operating speed. As a result, the simultaneous switching noise (SSN) induced by a large number of simultaneously switching circuits and the parasitic inductance of power/ground planes is becoming more and more serious [1]. It may affect sensitive circuits and its peak value may even cause logic failure. The power/ground planes play an important role in PDN to mitigate the SSN [2]. In the time domain, the power/ground planes not only perform as a high-frequency capacitor to provide charges to current loads in time, but also provide a return path for the current of signal lines. In the frequency domain, it is efficient to keep the impedance of PDN maintaining to a lower value over a wide frequency range. With the digital system's complexity increasing, the PDN is designed as a multilayered one in the printed circuit board (PCB) and packages. Transmission lines residing in different layers are interconnected by plated through-hole (PTH) vias. Due to the discontinuity of the return path of signals' return current, the return current will be coupled into the power/ground plane pairs, which may cause a resonant phenomenon in the power/ground plane pairs. In order to mitigate the noise coupled from the signal lines, the planes with the same reference voltage are stitched by vias, which can provide a low-impedance path to the return current [3].

Another important way to mitigate SSN is adding capacitors to PDN [4]–[7]. Capacitors work as a local charge library to provide charges to switching circuits in time. Hence a good decoupling design becomes very important to ensure a robust power distribution network in a high speed package/PCB. In the decoupling design, the power distribution network is first modeled from the IC power-supplying port to the voltage regulator modules (VRM) on the printed circuit board [5]. Then, according to the constraint of target impedance, appropriate capacitors are chosen to reduce the self-impedance of IC power-supplying port. But, the selection of decoupling capacitor is very complex. As a result, several auto-decoupling design methods were presented, such as the big 'V' [4], decade methods [5] and swarm intelligence

algorithms (Genetic Algorithm [6], Particle Swarm optimization, Cuckoo Search Method, and Firefly Algorithm [7]). In these auto-decoupling design methods, the decoupling design is a continuous iterative process until the self-impedance of the power-supplying port less than the target impedance in the frequency of interest. The model for the PDN not only should have a high accuracy, but also can be easily used to do numerical calculation. In previous work, power/ground planes were modeled as lumping capacitive elements in the decoupling design [8]. However, as clock frequency increases to gigahertz, the behaviors of the power/ground plane pairs that support the propagation of radial waves become more complex [9]. The lumping model becomes insufficient to characterize the features of the power/ground planes at high frequency. In addition, for the lumped PDN model, it is impossible to consider the influence of decoupling capacitors' placements to the performance of PDN. Hence, a precise model of power/ground planes that can exactly characterize its high-frequency performance becomes more important.

Nowadays, many methods have been presented to model the power/ground planes [10]–[13], such as partial element equivalent circuit (PEEC), multilayer finite element method (MFEM), Method of Moment (MOM) and Finite Difference Time Domain (FDTD). Although these methods can be applied exactly to model the power/ground planes, they are too time-consuming. The theoretical expression of the resonant cavity model is one of the fasted methods obtained by solving the 2-D Helmholtz wave equation for a rectangular plane pair [14]. The accuracy and the efficiency of this algorithm has been discussed by correlating with S-parameter measurements [15], [16]. In addition, several works [17]–[19] has been made to improve the poor convergence of the resonant cavity algorithm due to its double-infinite series. Another drawback of this algorithm is that it can only be applied to the regular power/ground planes without load circuits. In [20], the closed theoretical expression for the power/ground planes with single-port load circuits was deduced which extends the application scope of the resonant cavity algorithm. By being combined with the segmentation method and the inverted composition method, the application of the resonant cavity algorithm is extended to model the irregular shaped power/ground planes with single-port loads [20], [21]. But the modeling method in [20] is limited to the simple two-layered structure. In [22], a modeling method for the multilayered structure was presented. In this paper, the multilayered structure is decomposed into many single plane pairs. The single plane pairs is modeled firstly and then the equivalent model for the multilayered structure is obtained by connecting all the circuit models of the single plane pairs. By contrast, the modeling method presented in this paper takes the multilayered power/ground planes as a whole.

In this paper, the modeling method for the multilayered power/ground planes with stitching vias is presented on the basis of the resonant cavity algorithm. Firstly, the arrangements of the power/ground planes in a layer stack with mixed reference planes are divided into two basic units: adjacent planes with different reference voltage and that with the same reference voltage. Then, the return path of the switching current in the multilayered structure where some adjacent planes with different reference voltage is analyzed. On the basis of the return current path, the physics-based model for the multilayered structure is presented. Through analyzing the physics-based model, It is obtained that the remainder plane pairs act as a multiport load to the plane pair where the current load is located on. Next, the modeling method for the power/ground plane pair with multiport loads is presented to model the multilayered structure. In order to simplify the derivation process, the multiport load is replaced by a π-type circuit model to deduce the relationship between the voltages across the ports of the multiport load and the currents flowing into the load's ports. Finally, several examples are presented to validate the accuracy of this modeling method through the feature selective validation (FSV) method. This method not only has a high accuracy, but also had a high calculation speed. More importantly, this modeling method can be used as a basic algorithm in the auto-decoupling design. The advantage of this modeling method is that it can consider the influence of decoupling capacitor's placements in the auto-decoupling design. However, due to the limit of the resonant cavity algorithm [9], the modeling method is incapable of dealing with the structure of completely arbitrary shape.

This paper is organized as follows. In Section II, the return path of switching current in a multilayered power/ground planes is analyzed and the physics-based circuit model for multilayered power/ground planes is presented. In Section III, the modeling method for the power/ground planes with multiport loads is presented on the basis of the resonant cavity theory. In Section IV the accuracy of the modeling method is validated by several cases. In Section V, some specific conclusions are summarized.

II. PHYSICS-BASED MODEL FOR MULTILAYERED POWER/GROUND PLANE

According to different design requirements, there are different arrangements of power and ground planes in a multilayered stack. A multilayered structure can be seen as a combination of two basic units: adjacent planes with different reference voltage and that with the same reference voltage. The return current has different behaviors in the power/ground planes with different basic units.

A. CURRENT BEHAVIORS IN A MULTILAYERED STRUCTURE WHERE ADJACENT PLANES WITH DIFFERENT REFERENCE VOLTAGE

A simple four-layer structure with stitching vias is shown in Fig. 1(a). The current drawn or released by the switching circuits can be represented as a vertical current source. The power/ground plane pair can be considered as a dielectric resonant cavity with a PEC bottom wall and a PEC top wall.

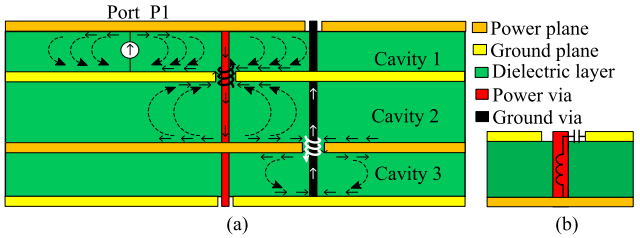

FIGURE 1. Multilayered power/ground planes (a) Multilayered power/ground planes where adjacent planes with different reference voltage (b) via capacitance and inductance definition for a via segment.

The propagation of the return current is confined in the region between planes at frequency above 10MHz because the skin depth is thinner than the PDN copper planes [9]. However, in the structure, shown in Fig. 1(a), the return current in one plane pair will propagate into another plane pair through the anti-paid of stitching vias.

When the vertical current source releases current to the PDN, the return current spreads out on the inner surfaces of the first plane and a large part of current return through the plane-to-plane distributed impedance and the ground via. A small part of the current will propagate into the second cavity through the power via. A large part of current on the above surface of the third plane will return to the below surface of the second plane through the plane-to-plane distributed impedance, and then snake around and change surfaces on the same plane. A small part of the current on the above surface of the third plane will snake around and transmit to the above surface of the fourth plane. Then, the current return to the below surface of the second plane through ground vias and return to the current source through the anti-pad of power vias. The return path of return current is shown in Fig. 1(a).

For the physics-based model of the four-layer structure, as shown in Fig. 1(b), the via barrel and the anti-pad are modeled by the inductor and capacitor, respectively, and the plane pairs are modeled by the resonant cavity algorithm. After connecting all the circuit models, the physics-based model of the multilayer PDN with stitching vias is extracted as shown in Fig. 2. The models of power vias and ground vias are connected by the red solid-line and the black dot-line, respectively. The 'via1-4'and 'ref1-4' represent the locations of the vias on the power and ground planes. The anti-pad parasitic capacitors that are public elements between two resonant cavities make the electrical characteristics of this model more complex.

From the analysis of the return path of the switching current, it is obtained that, the remainder plane pairs act as a multiport load to the first plane pair. The third cavities, ground stitching vias, and the via-stub of power stitching via in Fig. 3(a) can be equivalent to a two-port load, marked as "Load1", attached to the second cavity as shown in Fig. 3(b). The number of the load's port depends on the number of ground stitching via. The circuit in Fig. 3(b) can also be equivalent to a two-port network attached to the first cavity.

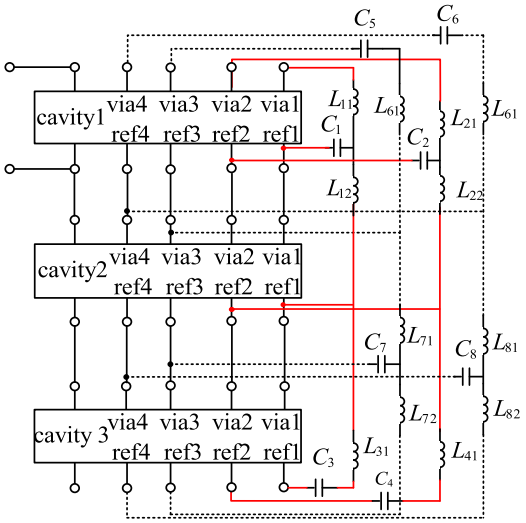

FIGURE 2. Physics-based circuit model for the multilayered structure.

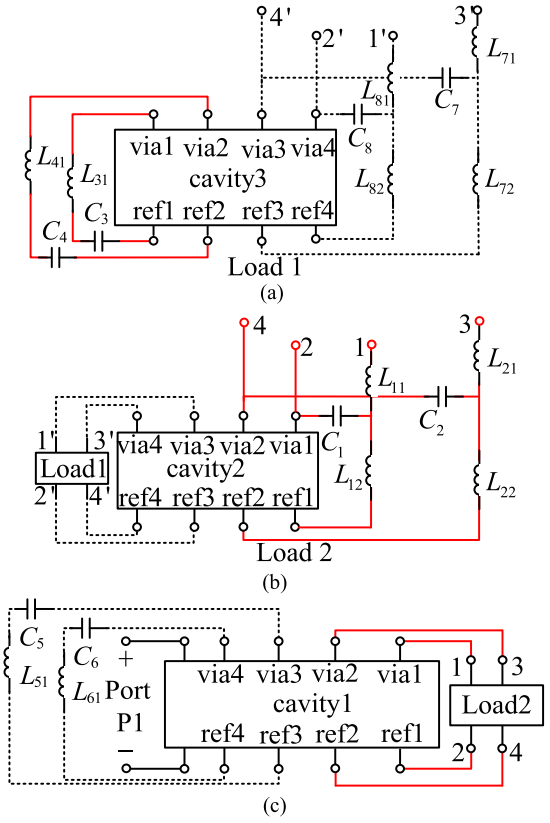

FIGURE 3. Simplified circuit model (a) Circuit model for the two-port network "Load1" (b) Circuit model for the two-port network "Load2" (c) Simplified circuit model for the physics-based circuit model.

The number of the load's port depends on the number of power stitching via. The equivalent circuit model for the multilayer PDN in Fig. 2 is shown in Fig. 3(c). The circuit model for the two port network "Load2" is shown in Fig. 3(b) which contains the second cavity, power stitching, the third cavity and ground stitching vias.

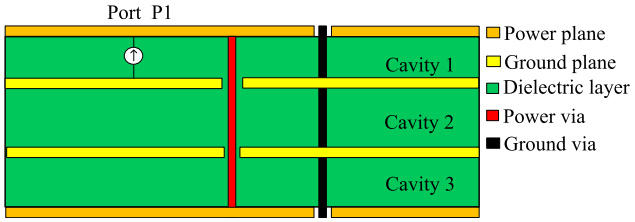

FIGURE 4. Multilayered power/ground planes where adjacent planes with the same reference voltage.

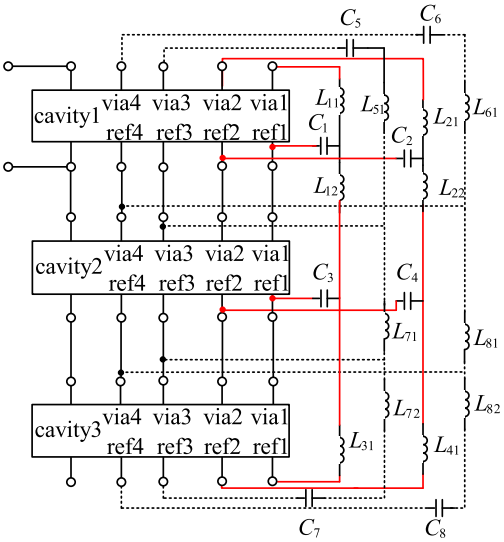

FIGURE 5. Physics-based circuit model for the multilayered structure in Fig. 4.

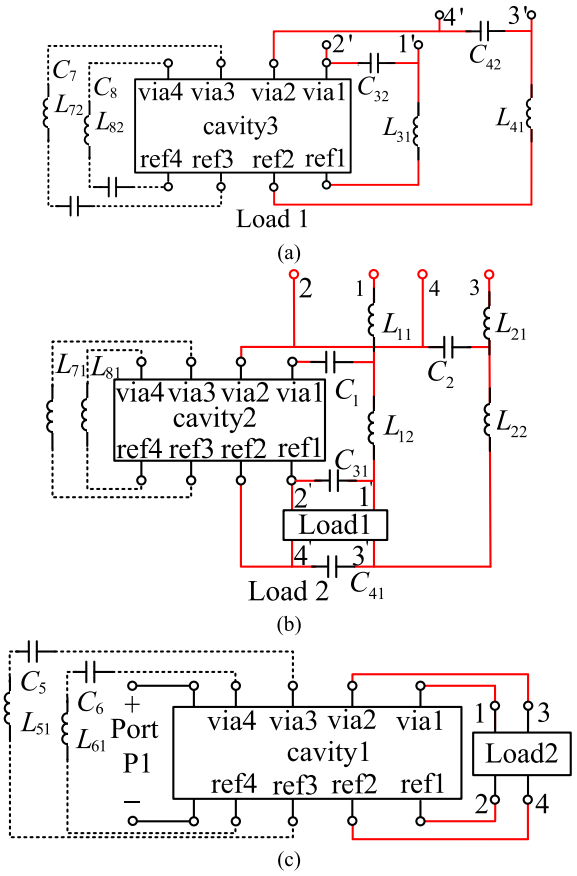

FIGURE 6. Simplified circuit model (a) Circuit model for the two-port network "Load1" (b) Circuit model for the two-port network "Load2" (c) Simplified circuit model for the physics-based circuit model.

B. PHYSICS-BASED MODEL FOR A MULTILAYERED STRUCTURE WITH ADJACENT PLANES WITH THE SAME REFERENCE VOLTAGE

The multilayered PDN in which some adjacent planes with the same reference voltage is shown in Fig. 4. The second and the third plane are the adjacent planes with the same reference voltage. The physics model of the multilayer PDN is shown in Fig. 5. The via barrel and the anti-pad are modeled by the inductor and capacitor, respectively. The models of power vias and ground vias are connected by the red solid-line and the black dot-line, respectively. The plane pairs are modeled by the resonant cavity method. Since three cavities are connected by the anti-pad capacitors of the power stitching via as a whole, the method of cascade network is used to analyze this multilayered structure. The anti-pad capacitance are divided into two parts and each of them is assigned to different plane pair. Take the anti-pad capacitors C3 as an example. These anti-pad capacitors connect the second and third cavity as a whole. The anti-pad capacitors C3 are divided into two parts C31 and C32. The capacitor C31 is assigned to the second cavity and the capacitor C32 is assigned to the third cavity. The ratio of the upper capacitance C31 to the lower capacitance C32 is equal to the ratio of the lower cavity's dielectric thickness to that of the upper cavity. The equivalent model for the third cavity and the power/ground stitching vias is shown in Fig. 6(a). It can be seen as a multiport load for the second cavity and it is connected to the upper anti-pad capacitors as shown in Fig. 6(b), which can be simplified as a multiport circuit with a multiport load. The equivalent circuit model for the multilayered PDN in Fig. 4 is shown in Fig. 6(c). It is the same as the final equivalent circuit of the structure whose adjacent planes are with different reference voltage. In a multilayered structure, it is can be seen the combination of these two basic units. Through above analysis, it is obtained that the task of modeling a multilayered structure can be simplified as that modeling a power/ground pair with multiport loads.

III. MODELING A POWER/GROUND PLANE WITH MULTIPORT LOAD

Based on the resonant cavity model, the modeling method for the power/ground planes pair with multiport loads is presented.

A. RESONANT CAVITY EQUATION

The propagation features of the power/ground planes are usually described as the self or transfer impedance. The resonant cavity equation can be used to efficiently compute the self and transfer impedance of a power/ground plane pair.

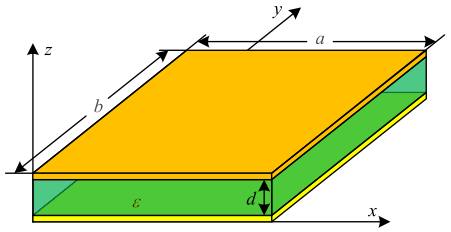

FIGURE 7. Structure for a simple power/ground plane pair.

Consider the plane structure in Fig. 7, which contains of two planes of dimensions $a \times b$, separated by a dielectric of thickness d. The dielectric constant is ε. This structure can be considered as a dielectric resonant cavity with a perfect electrical conductor (PEC) bottom wall and a PEC top wall. Since the plane spacing d is far smaller than λ(the wavelength) and $a, b \gg d$, the TM modes have 0 mode number along the z direction. The three main field components are Ez, Hx, and Hy. "E" is the electric field; "H" is the magnetic field; the subscripts represent the field direction. Because the boundary conditions along four sidewalls of the resonant cavity are assumed to be perfect magnetic conductor boundaries, the impedance matrix of a power/ground plane pair at two arbitrary ports can be computed by the resonant cavity algorithm:

$$Z_{ij}(\omega) = \frac{j\omega\mu d}{ab} \sum_{n=0}^{\infty} \sum_{m=0}^{\infty} \frac{\varepsilon_n^2 \varepsilon_m^2 f(x_i, y_i, x_j, y_j)}{k_{mn}^2 - k^2} \tag{1}$$

where d is the thickness of the dielectric between the two planes; a and b represent the plane dimensions; m and n are propagating modes; $\varepsilon_n, \varepsilon_m = 1$, for $n, m = 0$ and $\sqrt{2}$, otherwise;

$$\begin{aligned} f(x_i, y_i, x_j, y_j) &= \cos(\frac{m\pi x_i}{a})\mathrm{sinc}(\frac{m\pi t_{xi}}{2a})\cos(\frac{n\pi y_i}{b})\mathrm{sinc}(\frac{n\pi t_{yi}}{2b}) \\ &\quad \times \cos(\frac{m\pi x_j}{a})\mathrm{sinc}(\frac{m\pi t_{xj}}{2a})\cos(\frac{n\pi y_j}{b})\mathrm{sinc}(\frac{n\pi t_{yj}}{2b}) \end{aligned} \tag{2}$$

$$k_{mn} = \left(\frac{m\pi}{a}\right)^2 + \left(\frac{n\pi}{b}\right)^2 \tag{3}$$

$$k = k' - jk'' = \omega\sqrt{\varepsilon\mu} - j(\omega\sqrt{\varepsilon\mu}(\tan\delta + r/d)/2) \tag{4}$$

$$r = \sqrt{\frac{2}{\omega\mu\sigma}} \tag{5}$$

δ is the dielectric loss angle; r is the skin depth; (t_{xi}, t_{yi}) and (t_{xj}, t_{yj}) are the coordinates of the ports; (t_{xi}, t_{yi}) and (t_{xj}, t_{yj}) are port dimensions.

Assume $k'' \gg k'$ and $k_{mn} = 2\pi f_{mn}\sqrt{\varepsilon\mu}$, Equation (1) can be rewritten as:

$$Z_{ij}(\omega) = \sum_{n=0}^{\infty} \sum_{m=0}^{\infty} \frac{N_{mni} M_{mnj}}{j\omega C_{mn} + 1/j\omega L_{mn} + G_{mn}} \tag{6}$$

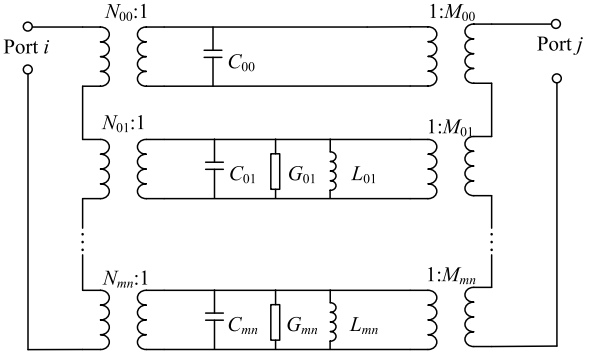

FIGURE 8. Resonant cavity circuit model for power/ground plane pair.

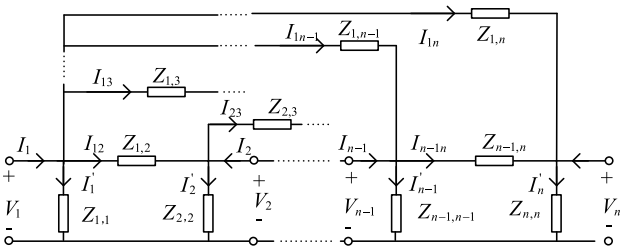

FIGURE 9. Equivalent π-type circuit model for a n-port network.

where

$$f_{mn} = \sqrt{(m/a)^2 + (n/b)^2}/2\sqrt{\varepsilon\mu} \tag{7}$$

$$N_{mni} = \varepsilon_m\varepsilon_n \cos\frac{m\pi x_i}{a}\mathrm{sinc}\frac{m\pi t_{xi}}{2a}\cos\frac{n\pi y_i}{b}\mathrm{sinc}\frac{n\pi t_{yi}}{2b} \tag{8}$$

$$M_{mnj} = \varepsilon_m\varepsilon_n \cos\frac{m\pi x_j}{a}\mathrm{sinc}\frac{m\pi t_{xj}}{2a}\cos\frac{n\pi y_j}{b}\mathrm{sinc}\frac{n\pi t_{yj}}{2b} \tag{9}$$

$$C_{mn} = \frac{\varepsilon ab}{d} \tag{10}$$

$$L_{mn} = \frac{d}{\varepsilon ab(2\pi f_{mn})^2} \tag{11}$$

$$G_{mn} = \frac{2\pi f C_{mn}(1 + d\tan\delta\sqrt{\pi f\mu\sigma})}{d\sqrt{\pi f\mu\sigma}} \tag{12}$$

The resonant cavity circuit model of the power/ground planes is shown in Fig. 8. Although it has a high efficiency, it can be seen from (6) that the resonant cavity equation has a poor convergence due to its double-infinite series. A fast algorithm, double-frequency approximation method (DFA) in [19], was presented to improve its convergence. In this fast algorithm, the propagating modes whose resonant frequency beyond the frequency range of interest are represented by an LC parallel circuit. Then, the power/ground planes pair can be modeled by the resonant cavity model with a certain number of propagating modes. In Section II, it is obtained that the remainder plane pairs can be seen as a multiport load for the plane pair where the current load is located on. In order to simplify the derivation process, the multiport load is replaced by a π-type circuit model, as shown in Fig. 9. The expression of the elements in the equivalence π-type circuit model is deduced as follows.

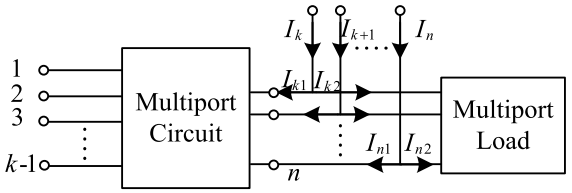

FIGURE 10. Diagram for a multiport circuit with a multiport load.

B. EQUIVALEN π-TYPE CIRCUIT MODEL FOR A MULIPORT LOAD

The equivalent π-type circuit model for a n-port load is shown in Fig. 9. The impedance matrix of the n-port network is shown as follows.

$$Z_{n-port} = \begin{pmatrix} V_1 \\ V_2 \\ \vdots \\ V_n \end{pmatrix} \begin{pmatrix} \frac{1}{I_1} & \frac{1}{I_2} & \cdots & \frac{1}{I_n} \end{pmatrix} = \begin{pmatrix} Z_{11} & Z_{12} & \cdots & Z_{1n} \\ Z_{21} & Z_{22} & \cdots & Z_{2n} \\ \vdots & \vdots & \ddots & \vdots \\ Z_{n1} & Z_{n2} & \cdots & Z_{nn} \end{pmatrix} \tag{13}$$

where V_i and I_i $(i = 1, 2, \ldots, n)$ are the port voltages and port currents of the π-type circuit. Through Kirchhoff's current law, the relationship between the port currents and port voltages is obtained as follows:

$$\begin{aligned} I_1 &= \frac{V_1}{Z_{1,1}} + \frac{V_1 - V_2}{Z_{1,2}} + \frac{V_1 - V_3}{Z_{1,3}} + \cdots + \frac{V_1 - V_n}{Z_{1,n}} \\ I_2 &= \frac{V_2}{Z_{2,2}} + \frac{V_2 - V_1}{Z_{1,2}} + \frac{V_2 - V_3}{Z_{1,3}} + \cdots + \frac{V_2 - V_n}{Z_{1,n}} \\ &\vdots \\ I_n &= \frac{V_n}{Z_{n,n}} + \frac{V_n - V_1}{Z_{1,2}} + \frac{V_n - V_2}{Z_{1,2}} + \cdots + \frac{V_n - V_{n-1}}{Z_{1,n-1}} \end{aligned} \tag{14}$$

where the impedance $Z_{i,j}$ is equal to $Z_{i,j}$ $(i, j = 1$ to $n)$. Equation (14) can be rewritten as follows after being rearranged:

$$\begin{pmatrix} I_1 \\ I_2 \\ \vdots \\ I_n \end{pmatrix} = \begin{pmatrix} \sum_{k=1}^{n} \frac{1}{Z_{1,k}} & -\frac{1}{Z_{1,2}} & \cdots & -\frac{1}{Z_{1,n}} \\ -\frac{1}{Z_{2,1}} & \sum_{k=1}^{n} \frac{1}{Z_{2,k}} & \cdots & -\frac{1}{Z_{2,n}} \\ \vdots & \vdots & \ddots & \vdots \\ -\frac{1}{Z_{n,1}} & -\frac{1}{Z_{n,2}} & \cdots & \sum_{k=1}^{n} \frac{1}{Z_{n,k}} \end{pmatrix} \begin{pmatrix} V_1 \\ V_2 \\ \vdots \\ V_n \end{pmatrix} \tag{15}$$

The relationship between the impedance matrix of the n-port load and the impedance of the elements in the π-type circuit model is shown as follows:

$$\begin{pmatrix} Z_{11} & Z_{12} & \cdots & Z_{1n} \\ Z_{21} & Z_{22} & \cdots & Z_{2n} \\ \vdots & \vdots & \ddots & \vdots \\ Z_{n1} & Z_{n2} & \cdots & Z_{nn} \end{pmatrix} = \begin{pmatrix} \sum_{k=1}^{n} \frac{1}{Z_{1,k}} & -\frac{1}{Z_{1,2}} & \cdots & -\frac{1}{Z_{1,n}} \\ -\frac{1}{Z_{2,1}} & \sum_{k=1}^{n} \frac{1}{Z_{2,k}} & \cdots & -\frac{1}{Z_{2,n}} \\ \vdots & \vdots & \ddots & \vdots \\ -\frac{1}{Z_{n,1}} & -\frac{1}{Z_{n,2}} & \cdots & \sum_{k=1}^{n} \frac{1}{Z_{n,k}} \end{pmatrix}^{-1} \tag{16}$$

The expression of the impedance of the elements in the π-type circuit model is shown as following equation:

$$\begin{pmatrix} Z_{1,1} & Z_{1,2} & \cdots & Z_{1,n} \\ Z_{2,1} & Z_{2,2} & \cdots & Z_{2,n} \\ \vdots & \vdots & \ddots & \vdots \\ Z_{n,1} & Z_{n,2} & \cdots & Z_{n,n} \end{pmatrix} = \begin{pmatrix} \frac{1}{\sum_{k=1}^{n} Y_{1k}} & -\frac{1}{Y_{12}} & \cdots & -\frac{1}{Y_{1n}} \\ -\frac{1}{Y_{21}} & \frac{1}{\sum_{k=1}^{n} Y_{2k}} & \cdots & -\frac{1}{Y_{2n}} \\ \vdots & \vdots & \ddots & \vdots \\ -\frac{1}{Y_{n1}} & -\frac{1}{Y_{n2}} & \cdots & \frac{1}{\sum_{k=1}^{n} Y_{nk}} \end{pmatrix} \tag{17}$$

where $Y_{i,j}$ $(i, j = 1$ to $n)$ is the element of the conductance matrix of the n-port network.

C. ALGORITHM FOR THE MULTIPORT CIRCUIT WITH A MULTIPORT LOAD

For the multilayered power/ground planes where some adjacent planes with the same reference voltage, the circuit model for the planes with the same reference voltage can be equivalent to a multiport circuit with a multiport load, as shown in Fig. 6 (b). To deduce the expression of the circuit model in Fig. 6 (b), a simplified circuit diagram is shown in Fig. 10. Assume the load is connected to the multiport circuit's port k to port n. The currents flow into the ports $k, k+1, \ldots, n-1$, and n are divided between the circuit model and the load. Let the multiport circuit be presented as:

$$\mathbf{V} = \mathbf{Z}^{\mathbf{M}}\mathbf{I}^{\mathbf{M}} \tag{18}$$

where the voltage matrix $\mathbf{V}$ is the voltage across every point and $\mathrm{V} = [V_1, V_2, \ldots, V_k, \ldots, V_n]^{\mathrm{T}}$. The current matrix $\mathbf{I}^{\mathbf{M}}$ is

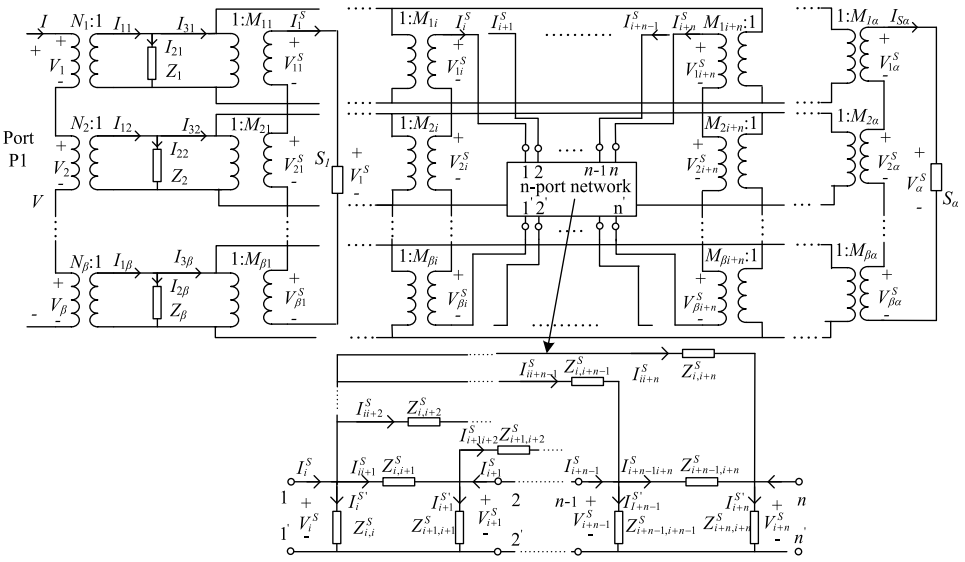

FIGURE 11. Resonant cavity circuit model for the power/ground plane with single-port loads and a *n*-port network.

the current flowing into each port of the *n*-port circuit model and $\mathrm{IM} = [I_1, I_2, \ldots, I_k, \ldots, I_n]^{\mathrm{T}}$. The expression of the impedance matrix $\mathbf{Z_M}$ is shown as follows.

$$\mathbf{Z^M} = \begin{pmatrix} Z_{11}^M & Z_{12}^M & \cdots & Z_{1k}^M & \cdots & Z_{1n}^M \\ Z_{21}^M & Z_{22}^M & \cdots & Z_{2k}^M & \cdots & Z_{2n}^M \\ \vdots & \vdots & \ddots & \vdots & \cdots & \vdots \\ Z_{k1}^M & Z_{k2}^M & \cdots & Z_{kk}^M & \vdots & Z_{kn}^M \\ \vdots & \vdots & \cdots & \vdots & \ddots & \vdots \\ Z_{n1}^M & Z_{n2}^M & \cdots & Z_{nk}^M & \cdots & Z_{nn}^M \end{pmatrix} \tag{19}$$

The relation between the current I_{h1} $(h = k, k+1, \ldots, n)$ flowing into the n-port circuit and that I_{h2} $(h = k, k+1, \ldots, n)$ flowing into the load is shown as follows:

$$I_{k1} = I_k - I_{k2}, I_{k+11} = I_k - I_{k+12}, \cdots, I_{n1} = I_n - I_{n2} \tag{20}$$

The current flowing into the load can be obtained by the **Y** parameter matrix and the port voltages of load, shown as follows.

$$\begin{pmatrix} I_{k2} \\ I_{k+12} \\ \vdots \\ I_{n2} \end{pmatrix} = \begin{pmatrix} Y_{11}^L & Y_{12}^L & \cdots & Y_{1k}^L \\ Y_{21}^L & Y_{22}^L & \cdots & Y_{2k}^L \\ \vdots & \vdots & \ddots & \vdots \\ Y_{k1}^L & Y_{k2}^L & \cdots & Y_{kk}^L \end{pmatrix} \begin{pmatrix} V_k \\ V_{k+1} \\ \vdots \\ V_n \end{pmatrix} \tag{21}$$

By substituting (20) and (21) into (18), V in (18) can be written as follows.

$$\mathbf{V} = \mathbf{Z^M I} - \mathbf{Z^M} * \mathbf{Y^L V} \tag{22}$$

$$\mathbf{Y^L} = \begin{pmatrix} 0 & 0 & \cdots & 0 & \cdots & 0 \\ 0 & 0 & \cdots & 0 & \cdots & 0 \\ \vdots & \vdots & \ddots & \vdots & \cdots & \vdots \\ 0 & 0 & \cdots & Y_{kk} & \vdots & Y_{kn} \\ \vdots & \vdots & \cdots & \vdots & \ddots & \vdots \\ 0 & 0 & \cdots & Y_{nk} & \cdots & Y_{nn} \end{pmatrix} \tag{23}$$

The impedance matrix $\mathbf{Z^W}$ for the *n*-port circuit with a multiport load can be written as follows by arranging (22).

$$\mathbf{Z^W} = (\mathbf{E_{n\times n}} + \mathbf{Z^M} * \mathbf{Y^L})^{-1} \mathbf{Z^M} \tag{24}$$

D. EQUATION FOR POWER/GROUND PLANES WITH A MULTIPORT LOAD

The resonant cavity circuit model for a power/ground plans pair with a π-type multiport load and single-port load is shown in Fig. 11. The number of the propagating modes of the resonant cavity circuit model is set as β according to the DFA fast modeling method. Variables used to deduce the self-impedance of the circuit model are also shown in Fig. 11.

By the Kirchhoff's current law, the expressions for the currents I_{1h} $(h = 1, 2, \cdots, \beta)$, flowing into each propagating mode, are obtained as follows.

$$\begin{aligned} I_{11} &= I_{21} + I_{31} \\ I_{12} &= I_{22} + I_{32} \\ &\vdots \\ I_{1\beta} &= I_{2\beta} + I_{3\beta} \end{aligned} \tag{25}$$

According to the property of the ideal transformer, the current I_{2h} and I_{3h} $(h = 1, 2, \ldots, \beta)$ can also be expressed as follows.

$$I_{2h} = \frac{V_h}{N_h Z_h} \quad (h = 1, 2, \cdots, \beta) \tag{26}$$

$$I_{3h} = M_{h1} I_1^S + M_{h2} I_2^S + \ldots + M_{h\alpha} I_\alpha^S \quad (h = 1, 2, \cdots, \beta) \tag{27}$$

Then, the expressions for the currents I_{1h} $(h = 1, 2, \cdots, \beta)$ can be rewritten as following equation.

$$\begin{aligned} I_{11} &= \frac{V_1}{N_1 Z_1} + M_{11} I_1^S + M_{12} I_2^S + \ldots + M_{1\alpha} I_\alpha^S \\ I_{12} &= \frac{V_2}{N_2 Z_2} + M_{21} I_1^S + M_{22} I_2^S + \ldots + M_{2\alpha} I_\alpha^S \\ &\vdots \\ I_{1\beta} &= \frac{V_\beta}{N_\beta Z_\beta} + M_{\beta 1} I_1^S + M_{\beta 2} I_2^S + \ldots + M_{\beta\alpha} I_\alpha^S \end{aligned} \tag{28}$$

where β is the total number of the propagating modes of the resonant cavity model and $\beta = (n + 1)(m + 1)$; Z_h, N_h and M_{hg} $(h = 1, 2, \cdots, \beta;\ g = 1, 2, \cdots, \alpha)$ are the mode impedance and port coefficients of the resonant cavity model. According to the property of the ideal transformer, the current I_{1h} $(h = 1, 2, \ldots, \beta)$ can also be expressed as follows.

$$I_{11} = N_1 I, I_{12} = N_2 I, \cdots, I_{1\beta} = N_\beta I \tag{29}$$

where I is the current flowing into the port P1. The expression of the current I_g^S, flowing into the single-port loads is shown as follows.

$$I_g^S = \frac{V_g^S}{Z_g^S} \quad (g = 1, 2, \cdots, \alpha;\ g \neq i, i+1, \ldots, i+n) \tag{30}$$

where Z_g^S and V_g^S $(g = 1, 2, \cdots, \alpha; g \neq i, i+1, \ldots, i+n)$ are the impedance of and the voltage across the gth single-port load S_g, respectively. The expression of the current flowing through the π-type multiport load is shown as follows.

$$I_g^S = I_g^{S'} + \sum_{j=0}^{n} I_{g,i+j}^S = \frac{V_g^S}{Z_g^S} + \sum_{j=0, i\neq g}^{n} \frac{V_g^S - V_{i+j}^S}{Z_{g,i+j}^S} \quad (g = i, i+1, \ldots, i+n) \tag{31}$$

where Z_g^S and $Z_{g,i+j}^S$ $(g = i, i+1, \ldots, i+n)$ are the impedance of the elements of the π-type multiport load. Variables I_g^S, $I_g^{S'}$, and V_g^S $(g = i, i+1, \ldots, i+n)$ are shown in Fig. 11. Equation (28) can be rewritten as (32), as shown at the top of the next page, by substituting (30) and (31) into it. By Kirchhoff's voltage law, the expressions for the voltages across the ports of each single-port load and the π-type n-port network are obtained as follows.

$$\begin{aligned} V_1^S &= V_{11}^S + V_{21}^S + \ldots + V_{\beta 1}^S \\ &= \frac{V_1 M_{11}}{N_1} + \frac{V_2 M_{21}}{N_2} + \ldots + \frac{V_\beta M_{\beta 1}}{N_\beta} \\ V_2^S &= V_{12}^S + V_{22}^S + \ldots + V_{\beta 2}^S \\ &= \frac{V_1 M_{12}}{N_1} + \frac{V_2 M_{22}}{N_2} + \ldots + \frac{V_\beta M_{\beta 2}}{N_\beta} \\ &\vdots \\ V_\alpha^S &= V_{1\alpha}^S + V_{2\alpha}^S + \ldots + V_{\beta\alpha}^S \\ &= \frac{V_1 M_{1\alpha}}{N_1} + \frac{V_2 M_{2\alpha}}{N_2} + \ldots + \frac{V_\beta M_{\beta\alpha}}{N_\beta} \end{aligned} \tag{33}$$

The relationship between the current I and voltage V_h $(h = 1, 2, \cdots, \beta)$ is obtained as follows by Substituting (29) and (33) into (32).

$$\begin{pmatrix} N_1 I \\ N_2 I \\ \vdots \\ N_\beta I \end{pmatrix} = A_{\beta\times\beta} \begin{pmatrix} \frac{V_1}{N_1} \\ \frac{V_2}{N_2} \\ \vdots \\ \frac{V_\beta}{N_\beta} \end{pmatrix} \tag{34}$$

where the parameter matrix $A_{\beta\times\beta}$ is expressed as (35), as shown at the top of the next page. Then, the expression of voltage V_h $(h = 1, 2, \cdots, \beta)$ can be presented as follows.

$$\begin{pmatrix} V_1 \\ V_2 \\ \vdots \\ V_\beta \end{pmatrix} = \begin{pmatrix} N_1 I \sum_{j=1}^{\beta} N_j A_{1j}^{-1} \\ N_2 I \sum_{j=1}^{\beta} N_j A_{2j}^{-1} \\ \vdots \\ N_\beta I \sum_{j=1}^{\beta} N_j A_{\beta j}^{-1} \end{pmatrix} \tag{36}$$

The self-impedance of port P1 is obtained as following equation.

$$Z_{11} = \frac{V_1 + V_2 + \cdots + V_\beta}{I} = \sum_{i=1}^{\beta} N_i \sum_{j=1}^{\beta} N_j A_{ij}^{-1} \tag{37}$$

where $A_{ij}^{-1}$is the element of the inverse matrix of the coefficient matrix $A_{\beta\times\beta}$. The trans-impedance between the port P1 and the gth load port is expressed as follows.

$$Z_{1g} = \sum_{i=1}^{\beta} M_{ig} \sum_{j=1}^{\beta} N_j A_{ij}^{-1} \quad (g = 1, 2, \ldots, \beta) \tag{38}$$

IV. EXAMPLE VALIDATION

The utilization of the modeling method is discussed based on the multilayered power/ground planes with through or blind stitching vias.

A. MULTILAYERED STRUCTURE WITH THROUGH VIAS

Consider a simple four-layer power distribution network with power and ground stitching vias as shown in Fig. 12. The adjacent planes are with different reference voltage. It contains of three plane pairs of dimensions 60 mm × 40mm separated by a dielectric of permittivity 4.4. There are four stitching vias located at (30 mm, 25mm), (34 mm, 25mm),

$$\begin{cases} I_{11} = \dfrac{V_1}{N_1 Z_1} + \dfrac{M_{11}V_1^S}{Z_1^S} + \dfrac{M_{12}V_2^S}{Z_2^S} + \ldots + M_{1i}\left(\dfrac{V_i^S}{Z_{i,i}^S} + \displaystyle\sum_{j=0,j\neq g}^{n} \dfrac{V_i^S - V_{i+j}^S}{Z_{i,i+j}^S}\right) + \cdots + M_{1i+n}\left(\dfrac{V_{i+n}^S}{Z_{i+n,i+n}^S} + \displaystyle\sum_{j=0,j\neq n}^{n} \dfrac{V_{i+n}^S - V_{i+j}^S}{Z_{i+n,i+j}^S}\right) \\ \quad + \ldots + \dfrac{M_{1\beta}V_\alpha^S}{Z_\alpha^S} \\ I_{12} = \dfrac{V_2}{N_2 Z_2} + \dfrac{M_{21}V_1^S}{Z_1^S} + \dfrac{M_{22}V_2^S}{Z_2^S} + \ldots + M_{2i}\left(\dfrac{V_i^S}{Z_{i,i}^S} + \displaystyle\sum_{j=0,j\neq g}^{n} \dfrac{V_i^S - V_{i+j}^S}{Z_{i,i+j}^S}\right) + \cdots + M_{2i+n}\left(\dfrac{V_{i+n}^S}{Z_{i+n,i+n}^S} + \displaystyle\sum_{j=0,j\neq n}^{n} \dfrac{V_{i+n}^S - V_{i+j}^S}{Z_{i+n,i+j}^S}\right) \\ \quad + \ldots + \dfrac{M_{2\beta}V_\alpha^S}{Z_\alpha^C} \\ \vdots \\ I_{1\beta} = \dfrac{V_\beta}{N_\beta Z_\beta} + \dfrac{M_{\beta 1}V_1^S}{Z_1^S} + \dfrac{M_{\beta 2}V_2^S}{Z_2^S} + \ldots + M_{\beta i}\left(\dfrac{V_i^S}{Z_{i,i}^S} + \displaystyle\sum_{j=0,j\neq g}^{n} \dfrac{V_i^S - V_{i+j}^S}{Z_{i,i+j}^S}\right) + \cdots + M_{\beta i+n}\left(\dfrac{V_{i+n}^S}{Z_{i+n,i+n}^S} + \displaystyle\sum_{j=0,j\neq n}^{n} \dfrac{V_{i+n}^S - V_{i+j}^S}{Z_{i+n,i+j}^S}\right) \\ \quad + \ldots + \dfrac{M_{\beta\beta}V_\alpha^S}{Z_\alpha^S} \end{cases} \tag{32}$$

$$A_{\beta\times\beta} = \begin{pmatrix} \dfrac{1}{Z_1} + \displaystyle\sum_{g=1}^{\alpha} \dfrac{M_{1g}^2}{Z_g^S} + \sum_{k=i}^{i+n} M_{1k} \sum_{j=0}^{n} \dfrac{M_{1k} - M_{1i+j}}{Z_{k,i+j}^S} & \displaystyle\sum_{g=1}^{\alpha} \dfrac{M_{1g}M_{2g}}{Z_g^S} + \sum_{k=i}^{i+n} M_{2k} \sum_{j=0}^{n} \dfrac{M_{1k} - M_{1i+j}}{Z_{k,i+j}^S} & \cdots & \displaystyle\sum_{g=1}^{\alpha} \dfrac{M_{1g}M_{\beta g}}{Z_g^S} + \sum_{k=i}^{i+n} M_{\beta k} \sum_{j=0}^{n} \dfrac{M_{1k} - M_{1i+j}}{Z_{k,i+j}^S} \\ \displaystyle\sum_{g=1}^{\alpha} \dfrac{M_{2g}M_{1g}}{Z_g^S} + \sum_{k=i}^{i+n} M_{1k} \sum_{j=0}^{n} \dfrac{M_{2k} - M_{2i+j}}{Z_{k,i+j}^S} & \dfrac{1}{Z_2} + \displaystyle\sum_{g=1}^{\alpha} \dfrac{M_{2g}^2}{Z_g^S} + \sum_{k=i}^{i+n} M_{2k} \sum_{j=0}^{n} \dfrac{M_{2k} - M_{2i+j}}{Z_{k,i+j}^S} & \cdots & \displaystyle\sum_{g=1}^{\alpha} \dfrac{M_{2g}M_{\beta g}}{Z_g^S} + \sum_{k=i}^{i+n} M_{\beta k} \sum_{j=0}^{n} \dfrac{M_{2k} - M_{2i+j}}{Z_{k,i+j}^S} \\ \vdots & \vdots & \ddots & \vdots \\ \displaystyle\sum_{g=1}^{\alpha} \dfrac{M_{\beta g}M_{1g}}{Z_g^S} + \sum_{k=i}^{i+n} M_{1k} \sum_{j=0}^{n} \dfrac{M_{\beta k} - M_{\beta i+j}}{Z_{k,i+j}^S} & \displaystyle\sum_{g=1}^{\alpha} \dfrac{M_{\beta g}M_{2g}}{Z_g^S} + \sum_{k=i}^{i+n} M_{2k} \sum_{j=0}^{n} \dfrac{M_{\beta k} - M_{\beta i+j}}{Z_{k,i+j}^S} & \cdots & \dfrac{1}{Z_\beta} + \displaystyle\sum_{g=1}^{\alpha} \dfrac{M_{\beta g}^2}{Z_g^S} + \sum_{k=i}^{i+n} M_{\beta k} \sum_{j=0}^{n} \dfrac{M_{\beta k} - M_{\beta i+j}}{Z_{k,i+j}^S} \end{pmatrix} \tag{35}$$

(32 mm, 21 mm), and (36 mm, 21 mm), respectively. The radii of the via and the anti-pad are 0.3 mm and 0.6 mm, respectively. Other parameters are shown in Fig. 12. The current drawn by switching circuits from the power distribution network is represented by a vertical current source that is located at (23 mm, 21 mm). The current in the first cavity flows into the second and the third resonant cavity through the anti-pad of the power and ground stitching vias. The cylindrical wave excited by the current source will cause a resonance in the second and third cavities, which influences the characteristics of the first cavity.

The physics-based circuit model for the structure in Fig. 12 is the same as that shown in Fig. 2. The via-stubs of power stitching vias, via1 and via 2, in the third cavity structure can be equivalent to single-port loads connected to the third cavity structure. The via-stubs of ground stitching vias, via 3 and via 4, in the first cavity structure can also be equivalent to single-port loads. The parasitic parameters of stitching vias, such as anti-pad capacitance and via barrel inductance, are extracted by ANSYS Q3D Extractor. The resonant cavity algorithm is used to compute the impedance of the power/ground plane. The self-impedances of port P1 in the frequency domain computed by (37) with different number of propagating modes and that simulated by commercial tool, High Frequency Structure Simulator (HFSS), are shown in Fig. 13.

It shows that the accuracy of (37) is improved as the number of propagating modes used to model the power/ground plane pair increases. The method, feature selective validation (FSV), is used to compare the self-impedance computed by (37) with that simulated by HFSS to see how similar the two data sets are [23]–[25]. The FSV method comprises three component measures: the amplitude difference measure (ADM) which is to compare amplitude, the feature difference measure (FDM) which is to compare the rapidly changing feature, and the global difference measure (GDM) which is combined by ADM and FDM. FSV interpretation for point-by-point ADM/FDM/ GDM value and six-point scale is shown in Table 1. The trends of the point-by-point ADM/FDM/GDM values with the number of the propagating mode are shown in Fig. 14. With the number of propagating modes used in (37) increasing, it can be observed that the accuracy of (37) is improved rapidly.

Good agreement can be seen for the self-HFSS to see how similar the two data sets are [23]–[25]. The FSV method comprises three component measures: the amplitude difference measure (ADM) which is to compare amplitude, the feature difference measure (FDM) which is to compare the rapidly

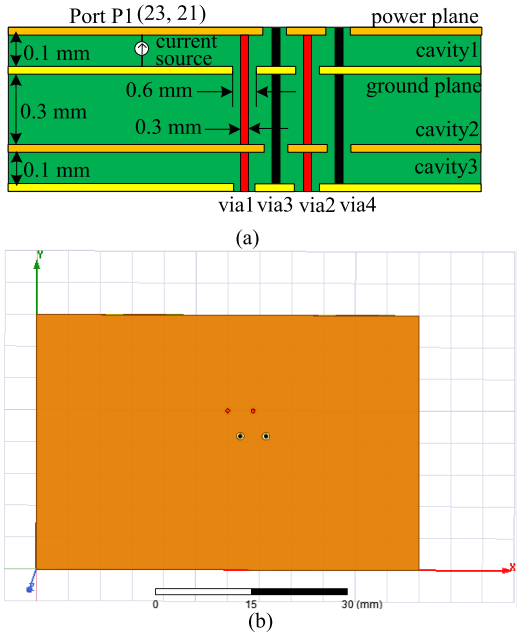

FIGURE 12. Multilayered structure where adjacent planes with different reference voltage (a)parameters of structure (b) structure in HFSS.

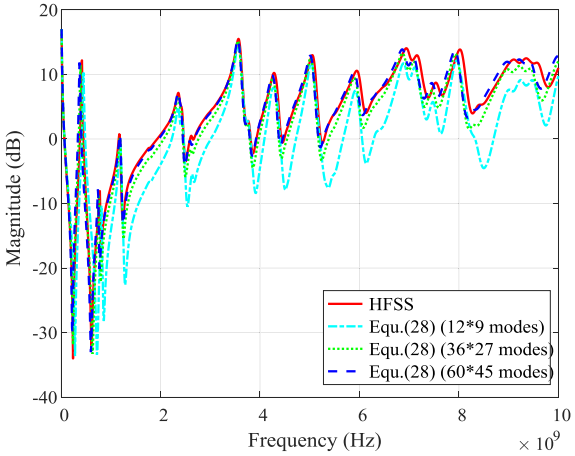

FIGURE 13. Self-impedance of port P1 on the multilayered structure.

TABLE 1. FSV interpretation scales.

ADM/FDM/GDM Value	FSV Interpretation	FSV Point Scale
Less than 0.1	EXCELLENT	1
Between 0.1 and 0.2	VERY GOOD	2
Between 0.2 and 0.4	GOOD	3
Between 0.4 and 0.8	FAIR	4
Between 0.8 and 1.6	POOR	5
Greater than 1.6	VERY POOR	6

changing feature, and the global difference measure (GDM) which is combined by ADM and FDM. FSV interpretation for point-by-point ADM/FDM/ GDM value and six-point scale is shown in Table 1. The trends of the point-by-point ADM/FDM/GDM values with the number of the propagating

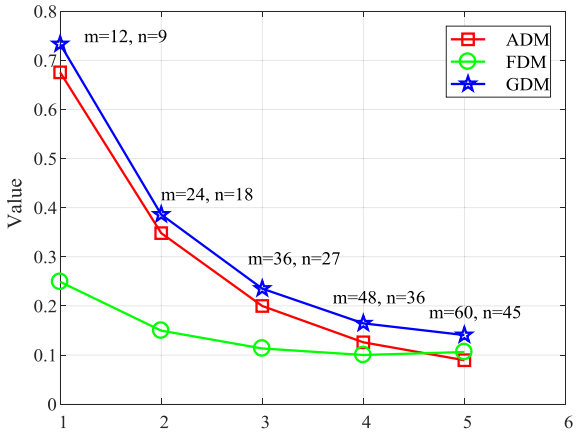

FIGURE 14. Grade-spread chart for the self-impedance of port P1.

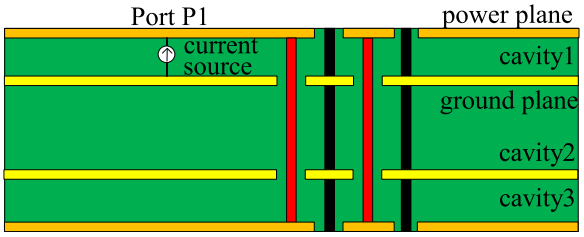

FIGURE 15. Multilayered Structure where some adjacent plane with the same reference voltage.

mode are shown in Fig. 14. With the number of propagating modes used in (37) increasing, it can be observed that the accuracy of (37) is improved rapidly. Good agreement can be seen for the self-impedance both in magnitude and phase. When the number of propagating modes is (60∗45), the ADM value even reaches to the "EXCELLENT" level.

However, It is also can be seen that, from Fig. 13, the error between the two data sets becomes lager at the frequency range higher than 7GHz. It is the influence of the bandwidth of the lumped LC equivalent circuit in the DFA algorithm that results to the variation of the accuracy at high frequency. The circuit structure where some adjacent planes are with the same reference voltage is shown in Fig. 15. The second and third plane are with the same reference voltage. Its physics-based circuit model is the same as that shown in Fig. 5. The structural parameters are the same as that in Fig. 12. The impedance of the multiport load consisting of the stitching vias and the second and third cavities is computed by (24). The self-impedances of port P1 in frequency domain computed by (37) with (60∗45) propagating modes and that simulated by HFSS are shown in Fig. 16. Good agreement can be seen from the comparison of the self-impedances. Due to the influence of the bandwidth of the LC equivalent circuit in the DFA algorithm, the accuracy of the algorithm varies at high frequency.

B. MULTILAYERED STRUCTURE WITH BLIND VIAS

Consider a simple five-layered power distribution network shown in Fig. 17 where the adjacent planes with

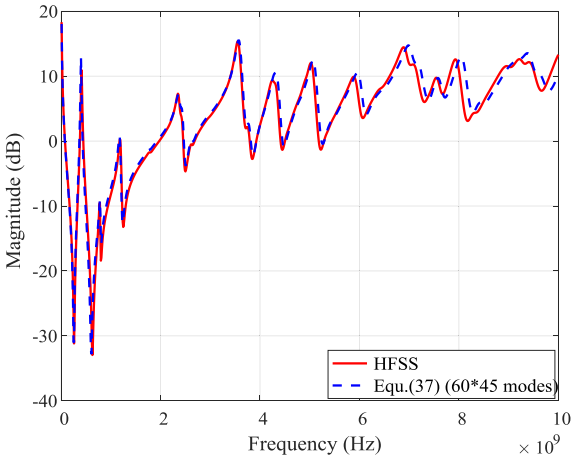

FIGURE 16. Self-impedance of port P1 on the multilayered structure where some adjacent planes with the same voltage.

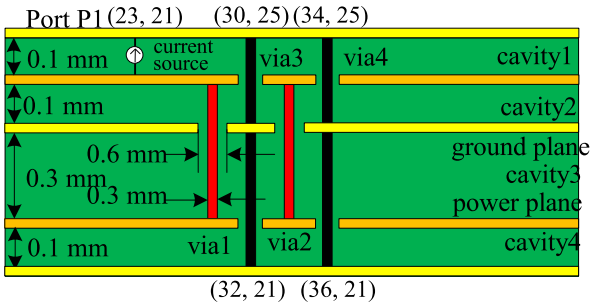

FIGURE 17. Multilayered Structure with blind power stitching vias.

different voltage. It contains of three ground planes and two power planes of dimensions 60 mm × 40mm separated by a dielectric of permittivity 4.4. There are four stitching vias located at (30 mm, 25 mm), (34 mm, 25 mm), (38 mm, 25 mm), (32 mm, 21 mm), (36 mm, 21 mm), and (40 mm, 21 mm), respectively. The current drawn by the switching circuits from the power distribution network is represented by a vertical current source and located at (23 mm, 21 mm). Other parameters are also shown in Fig. 17.

For this five-layered power distribution network, it is the combination of these two basic units: adjacent planes with different reference voltage and that with the same reference voltage. Since the power stitching vias are blind via, in the physics-based circuit model, there is only a multiport load connected to the first cavity. When computing the self-impedance of port P1, the current flowing into the single-port load in (32) should be ignored. The self-impedance of port P1 computed by (37) with (60∗45) propagating modes and that simulated by HFSS are shown in Fig. 18. Good agreement can be seen from the comparison of the self-impedances. However, due to the influence of the bandwidth of the LC equivalent circuit in the DFA algorithm, the accuracy of the algorithm varies at high frequency.

C. APPLICATION OF THIS MODELING METHOD IN DECOUPLING DESIGN

In high-speed circuit, decoupling capacitors play an important role in the power distribution network, which can

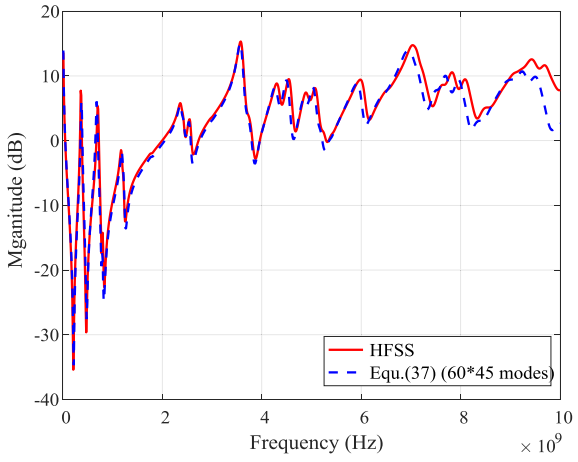

FIGURE 18. Self-impedance of port P1 on the multilayered structure with blind stitching vias.

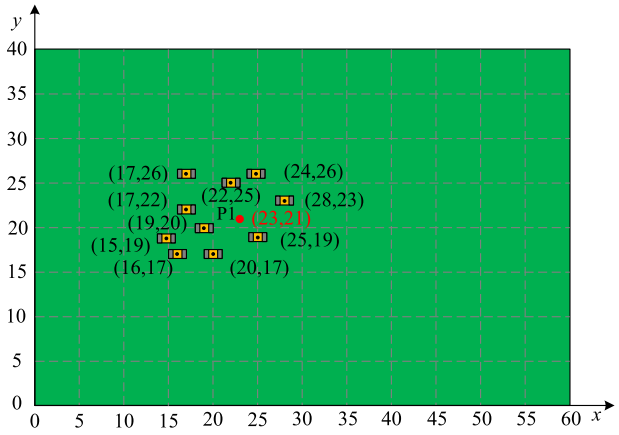

FIGURE 19. Locations of the Decoupling Capacitors Attached to the Plane Pair.

mitigate power noise efficiently through providing charges to the current load. As clock frequency increases, it becomes more and more important to help designers to understand the effect of decoupling capacitor and do some decoupling design efficiently. The purpose of this modeling method is to provide a basic algorithm for the auto-decoupling design for a multilayered PDN, which can consider the placements of decoupling capacitors.

A test case is developed to check the accuracy of this method to model the multilayered power/ground planes with decoupling capacitors. Ten decoupling capacitors are attached to the first cavity around the port 1. Each decoupling capacitor has a capacitance of 0.39 nF with 0.52 nH parasitic inductance and 0.5 Ohm parasitic resistance. Their locations on the first cavity are shown in Fig. 19. The impedance of port P1 is shown in Fig. 20. The comparison with the result simulated by HFSS illustrates the modeling method's accuracy for the multilayered structure with capacitors.

Compared with the self-impedance of the multilayered structure without decoupling capacitors, suppression of the resonant peaks in the multilayered structure with decoupling capacitors because of the capacitive nature of the capacitors

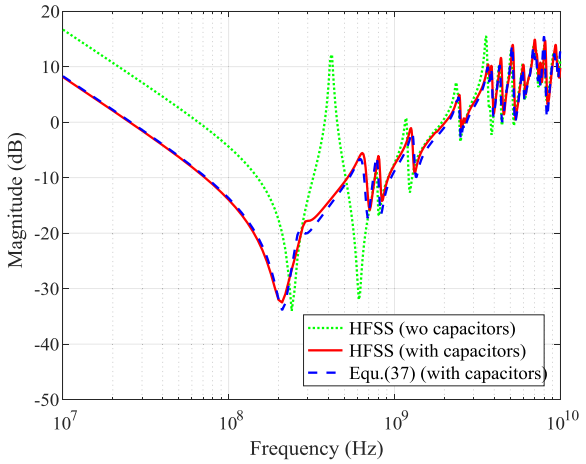

FIGURE 20. Self-impedance of port 1 on the multilayered structure with ten decoupling capacitors.

can be observed. The self-impedance of port P1 at low frequency is influenced by these decoupling capacitors. However, at high frequency, the impedance of port P1 is almost unchanged. Since the series resonant frequency of the decoupling capacitor (0.353 GHz) is too low to influence the impedance of port P1 at high frequency.

V. CONCLUSION

Based on the resonant cavity algorithm, a modeling method for the multilayered power/ground planes with stitching vias has been discussed in this paper. Firstly, the influence of the stitching vias to the return path of switching current is analyzed. It is the anti-pad capacitance that transforms the switching current to other cavities and connect the cavities as a whole. On the basis of the return current path, it is obtained that the remainder plane pairs act as a multiport load to the plane pair where the current load is located in. Then, this paper describes the physical principle, formulation, and implementation of the modeling method for multilayered power/ground planes. According to the different structure of multilayered planes and different types of stitching vias, the results computed by the modeling method presented in this paper are comprised with that simulated by HFSS. The FSV results show the accuracy of the modeling method. It is also demonstrated that the modeling method can be applied to solve the auto-decoupling design for a multilayered power/ground planes. The advantage of this modeling method is that it can consider the influence of decoupling capacitor's placements in the auto-decoupling design.

REFERENCES

[1] P. Gupta and A. B. Kahng, "Efficient design and analysis of robust power distribution meshes," in *Proc. 19th Int. Conf. Very Large Scale Integr. Design (VLSID)*, Jan. 2006, pp. 337–342.

[2] L. D. Smith, "Simultaneous switch noise and power plane bounce for CMOS technology," in *Proc. IEEE 8th Top. Meeting Elect. Perform. Electron. Packag.*, Oct. 1999, pp. 163–166.

[3] M.-S. Zhang, J.-F. Mao, and Y.-L. Long, "Power noise suppression using power-and-ground via pairs in multilayered printed circuit boards," *IEEE Trans. Compon., Packag., Manuf. Technol.*, vol. 1, no. 3, pp. 374–385, Mar. 2011.

[4] S. Weir, "Bypass filter design considerations for modern digital systems, a comparative evaluation of the big 'V,' multi-pole, and many pole bypass strategies," in *Proc. Design Conf.*, Santa Clara, CA, USA, Feb. 2006, pp. 1608–1630.

[5] L. D. Smith, R. E. Anderson, D. W. Forehand, T. J. Pelc, and T. Roy, "Power distribution system design methodology and capacitor selection for modern CMOS technology," *IEEE Trans. Adv. Packag.*, vol. 22, no. 3, pp. 284–291, Aug. 1999.

[6] K. Bharath, E. Engin, and M. Swaminathan, "Automatic package and board decoupling capacitor placement using genetic algorithms and M-FDM," in *Proc. 45th ACM/IEEE Design Autom. Conf. (DAC)*, Anaheim, CA, USA, Jun. 2008, pp. 560–565.

[7] J. N. Tripathi, N. K. Chhabra, R. K. Nagpal, R. Malik, and J. Mukherjee, "Damping the cavity-mode anti-resonances' peaks on a power plane by swarm intelligence algorithms," in *Proc. IEEE Int. Symp. Circuits Syst. (ISCAS)*, Seoul, South Korea, May 2012, pp. 361–364.

[8] J. Kim, K. Shringarpure, J. Fan, J. Kim, and J. L. Drewniak, "Equivalent circuit model for power bus design in multi-layer PCBs with via arrays," *IEEE Microw. Wireless Compon. Lett.*, vol. 21, no. 2, pp. 62–64, Feb. 2011.

[9] N. Na, J. Choi, S. Chun, M. Swaminathan, and J. Srinivasan, "Modeling and transient simulation of planes in electronic packages," *IEEE Trans. Adv. Packag.*, vol. 23, no. 3, pp. 340–352, Aug. 2000.

[10] A. E. Ruehli, "Equivalent circuit models for three-dimensional multiconductor systems," *IEEE Trans. Microw. Theory Techn.*, vol. MTT-22, no. 3, pp. 216–221, Mar. 1974.

[11] J. Y. Choi and M. Swaminathan, "Decoupling capacitor placement in power delivery networks using MFEM," *IEEE Trans. Compon., Packag., Manuf. Technol.*, vol. 1, no. 10, pp. 1651–1661, Oct. 2011.

[12] Y. Ji and T. H. Hubing, "On the modeling of a gapped power-bus structure using a hybrid FEM/MoM approach," *IEEE Trans. Electromagn. Compat.*, vol. 44, no. 4, pp. 566–569, Nov. 2002.

[13] J.-G. Yook, N. I. Dib, and L. P. B. Ratehi, "Characterization of high frequency interconnects using finite difference time domain and finite element methods," *IEEE Trans. Microw. Theory Techn.*, vol. 42, no. 9, pp. 1727–1736, Sep. 1994.

[14] T. Okoshi, *Planar Circuits for Microwaves and Lightwaves*. Munich, Germany: Springer-Verlag, 1984.

[15] G.-T. Lei, R. W. Techentin, P. R. Hayes, D. J. Schwab, and B. K. Gilbert, "Wave model solution to the ground/power plane noise problem," *IEEE Trans. Instrum. Meas.*, vol. 44, no. 2, pp. 300–303, Apr. 1995.

[16] N. Na and M. Swaminathan, "Modeling and transient simulation of planes in electronic packages for GHz systems," in *Proc. IEEE 18th Topical Meeting Elect. Perform. Electron. Packag.*, Oct. 1999, pp. 149–152.

[17] Z. L. Wang, O. Wada, Y. Toyota, and R. Koga, "Convergence acceleration and accuracy improvement in power bus impedance calculation with a fast algorithm using cavity modes," *IEEE Trans. Electromagn. Compat.*, vol. 47, no. 1, pp. 2–9, Feb. 2005.

[18] C. Wang *et al.*, "An efficient approach for power delivery network design with closed-form expressions for parasitic interconnect inductances," *IEEE Trans. Adv. Packag.*, vol. 29, no. 2, pp. 320–334, May 2006.

[19] J.-M. Lu, Y.-S. Li, and M.-S. Zhang, "An efficient SPICE-compatible cavity resonant model for microstrip lines," *IEEE Trans. Compon., Packag., Manuf. Technol.*, vol. 1, no. 4, pp. 574–585, Apr. 2011.

[20] J. Wang, J. Lu, X. Chu, Y. Liu, and Y. Li, "Modeling and simulation of planes with decoupling capacitors," *IEEE Trans. Compon., Packag., Manuf. Technol.*, vol. 6, no. 7, pp. 1087–1098, Jul. 2016.

[21] J. Wang, J. Lu, and Y. Li, "Placement of decoupling capacitor on packages based on effective decoupling radius," in *Proc. 18th IEEE Electron. Packag. Technol. Conf.*, Singapore, Nov./Dec. 2016, pp. 195–198.

[22] R. Rimolo-Donadio *et al.*, "Physics-based via and trace models for efficient link simulation on multilayer structures up to 40 GHz," *IEEE Trans. Microw. Theory Techn.*, vol. 57, no. 8, pp. 2072–2083, Aug. 2009.

[23] A. Orlandi, G. Antonini, C. Ritota, and A. P. Duffy, "Enhancing feature selective validation (FSV) interpretation of EMC/SI results with grade-spread," in *Proc. IEEE Int. Symp. Electromagn. Compat.*, vol. 2, Aug. 2006, pp. 362–367.

[24] *IEEE Standard for Validation of Computational Electromagnetics Computer Modeling and Simulations*, IEEE Standard 1597.1-2008, 2008.

[25] *IEEE Recommended Practice for Validation of Computational Electromagnetics Computer Modeling and Simulations*, IEEE Standard 1597.2-2010, 2011.

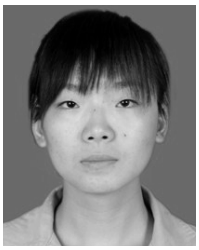

JUN WANG received the B.S. degree in electronic information science and technology from the Langfang Teachers College, Langfang, China, in 2008, and the D.Eng. degree from Xidian University, Xi'an, China, in 2017.

She is currently a Post-Doctoral Researcher with the Electronic and Engineering Institute, Xidian University. Her current research interests focus on signal integrity, jitter, and power integrity.

JIANMIN LU received the B.S. degree in material engineering from Zhengzhou University, Zhengzhou, China, in 2005, and the Ph.D. degree in electrical engineering from Xidian University, Xi'an, China, in 2012.

He is currently with the Institute of Electronic CAD affiliated with the Key Laboratory of High-Speed Circuit Design and EMC, Ministry of Education, Xidian University. His current research interests focus on power noise suppression, time-domain simulation, and high-speed interconnect modeling.

XIUQIN CHU received the M.Eng. and D.Eng. degrees from Xidian University, Xi'an, China, in 1997 and 2003, respectively.

She is currently an Associate Professor with the Electronic and Engineering Institute, Xidian University. Her main research interests are digital image processing and signal integrity.

YANG LIU received the M.Eng. and D.Eng. degrees from Xidian University, Xi'an, China, in 2004 in 2007, respectively.

He is currently an Associate Professor with the Electronic and Engineering Institute, Xidian University. His current research interests include power integrity, signal integrity, and image processing.

YUSHAN LI received the B.S. degree in electronic engineering from Harbin Engineering University, Harbin, China, in 1968, and the M.S.E. degree in electronic engineering from Xidian University, Xi'an, China, in 1981.

In 1981, he joined the School of Electronic Engineering, Xidian University, as a Faculty Member. From 1986 to 1987, he was a Visiting Scholar and a Research Associate with the Department of Electrical and Computer Engineering, University of Miami, Coral Gables, FL, USA. He is currently a Professor and a Ph.D. Candidate Advisor with the School of Electronic Engineering, Xidian University. His current research interests include electronic design automation and signal integrity analysis.